

Nanostructured Metal Films Formed onto Porous Silicon Template

Hanna Bandarenka^{1,a}, Alexei Dolgiy^{1,b}, Eugene Chubenko^{1,c}, Sergei Redko^{1,d},
Kseniya Girel^{1,e}, Serghej Prischepa^{1,f}, Andrei Panarin^{2,g}, Sergei Terekhov^{2,h},
Vladimir Pilipenko^{3,i}, and Vitaly Bondarenko^{1,j*}

¹Belarusian State University of Informatics and Radioelectronics,
6 Brovka st., Minsk 220013 Belarus

²B.I. Stepanov Institute of Physics, 68 Nezavisimosti ave, Minsk 220012 Belarus

³Research and Design Center "Belmicrosystems", INTEGRAL Joint Stock Company,
Kazintsa sq., Minsk 220064 Belarus

^ah.bandarenka@bsuir.by, ^bdolgiy@bsuir.by, ^ceugene.chubenko@bsuir.by, ^dsv.redko@bsuir.by
^ek.girel@bsuir.by, ^fprischepa@bsuir.by, ^ga.panarin@ifanbel.bas-net.by,
^hterekhov@imaph.bas-net.by, ⁱoffice@bms.by, ^jvitaly@bsuir.edu.by

Keywords: porous silicon, pattern inheritance, noble and transition metals, superconductivity, plasmon resonance, SERS, electroporation.

Abstract. The review reports results of our research work on nanostructured metal films on porous silicon. Principal steps of the techniques allowing fabrication of metal films completely inheriting morphological pattern of different types of porous silicon are presented. It is shown, that imprinting of the nanostructured pattern to metal films by means of porous silicon template opens their new structural, optical, mechanical and electrical properties, which can be successfully applied in nanoelectronics and biomedicine, particularly including devices based on superconductivity effect, SERS analysis with picomolar sensitivity and transdermal drug delivery by electroporation.

Introduction

Open structure of porous Si (PS) has driven scientists to introduce in its pores different "foreign" substances, such as metals, semiconductors, dielectrics, organic and biological species, pursuing a goal to create composite and hybrid materials with outstanding properties [1-7]. Figuratively speaking, under this approach PS plays a role of the "host" material, which takes the other one as a "guest". Among various prospective "guests" in PS, metals are some of very attractive ones due to their specific electrical, magnetic and optical properties. For many years, PS has been considered as a porous template for filling with metals by their deposition *into* the pore volume (Fig. 1). In this way, a controllable definition of dimensions and shapes of metal nanostructures has been achieved. For instance, in Fig. 1, b one can see that managing diameters of the pores provides formation of metal nanoparticles (NPs) of required sizes [2, 4, 5]. On the other hand, Fig. 1, c shows that metal nanowires (NWs) of a variable aspect ratio can be grown by deposition into elongated pores of PS [4-6]. However, the potential of PS as the porous template is not limited by the formation of the metal NPs or NWs. Recently, scientific community has turned an attention on PS as a tool for the nanostructuring of metal films by their deposition *onto* different parts of the surface of PS skeleton, i.e. rests of Si elements between the pores [7-16]. Combinations of the PS morphologies and methods of metal deposition give an opportunity to create the metal films with novel fascinating characteristics. Fig. 2 schematically illustrates types of the nanostructured metal films that can be grown on the PS templates. Actually, family of morphological types of PS is very rich. PS may look like a sponge or consist of vertical pore channels with branched or flat walls [17]. The pore diameters vary in wide ranges: less than 2 nm (microPS), between 2 and 50 nm (mesoPS) and more than 50 nm (macroPS) [18]. Here in Fig. 2 we have considered an example of the PS morphology typical for meso- and macroPS with the vertical pores. Such PS is a perfect candidate as the

template for nanostructuring of metal films, which would possess reproducible properties across a single sample and from sample to sample. The morphology of the metal film strongly depends on the deposition method and type of the PS template, while its properties are not usual for the bulk metals as hereinafter is shown.

The purpose of this review is to capture for reader the most important results on the routes of fabrication of the PS template and following metal deposition depending on the desired morphology of metal films, their properties and applicability prospects.

Technological Aspects of PS Fabrication

By nowadays many techniques of PS fabrication have been already introduced. PS destined for the nanostructuring of metal films has to be formed by the method which provides the desired pore diameter, thickness of the porous layer and dimensions of Si elements remaining between pores (the PS skeleton, Fig. 1, a). Moreover, it is very important to ensure uniformity and repeatability of such PS parameters.

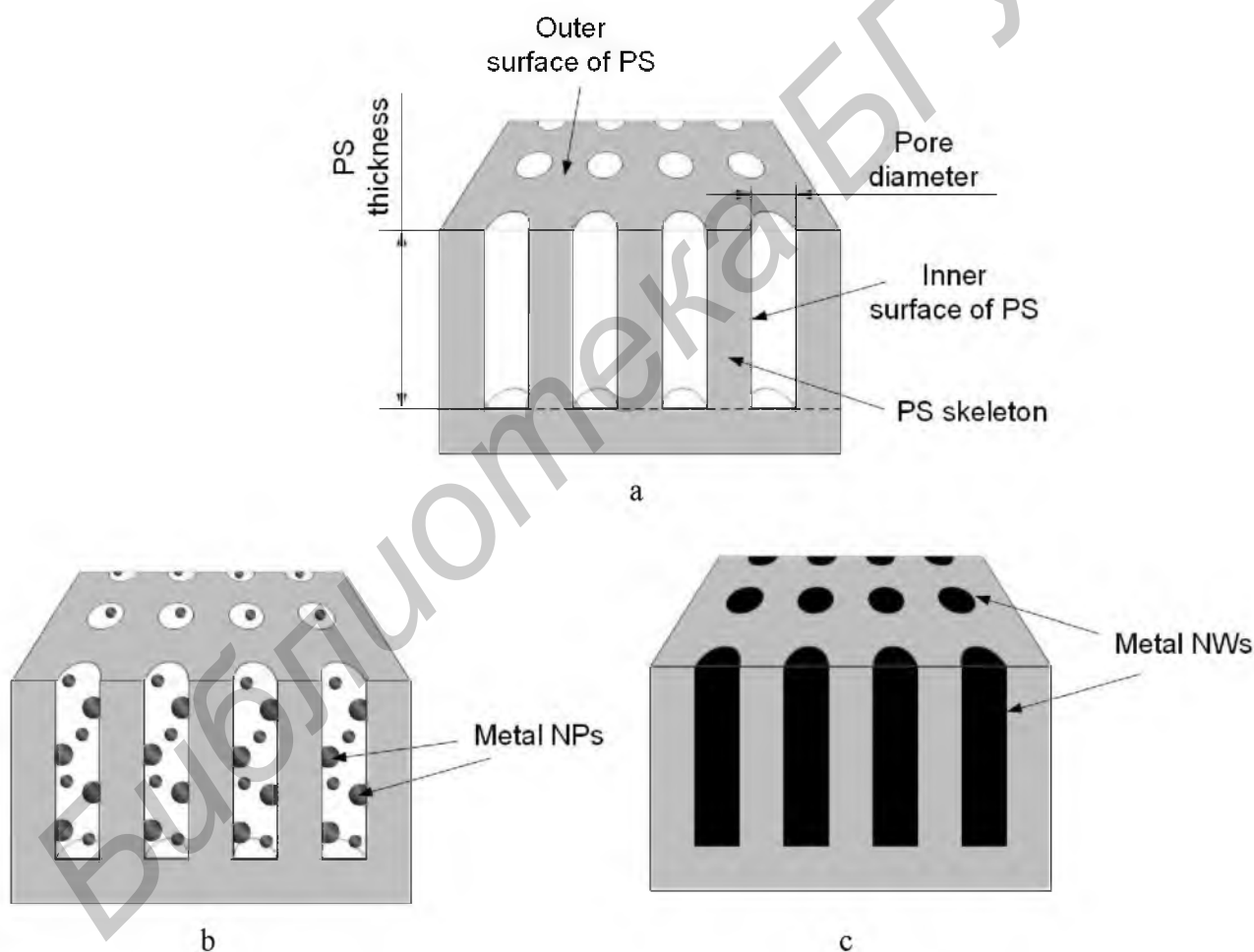


Fig. 1. Schematic illustration of (a) PS with definition of its structural parameters, (b) metal NPs and (c) metal NWs deposited *into* pores of PS

Thus, production of the PS templates is a specific process to control, and active investigations are currently underway to find possibilities of its improvement. In our works, we have used an electrochemical anodization of monocrystalline Si wafers in HF (hydrofluoric acid)-based solutions to form PS following the same fabrication procedure described elsewhere [19, 21].

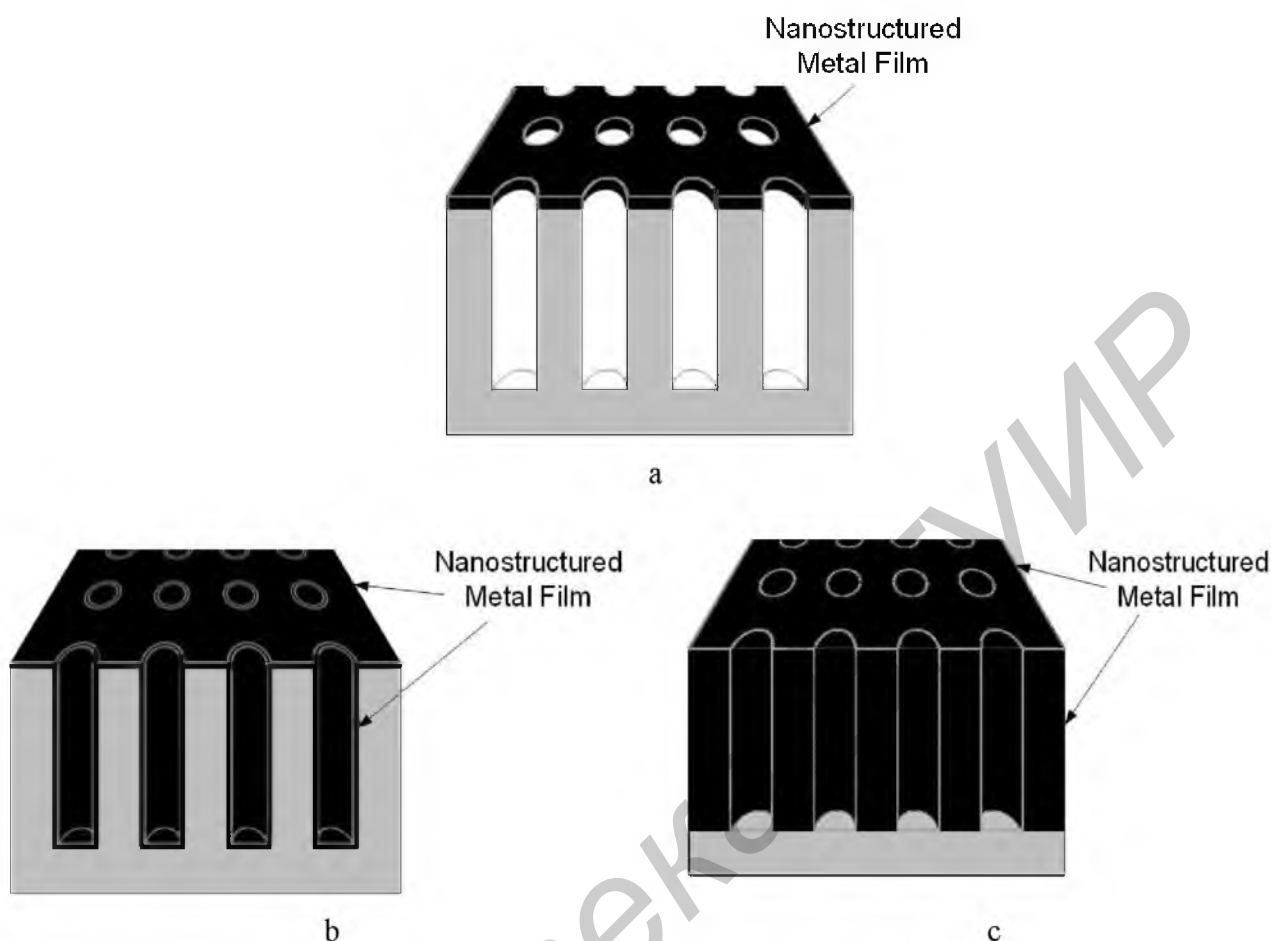


Fig. 2. Schematic illustration of nanostructured metal films deposited *onto* (a) outer, (b, c) outer and inner surfaces of PS; (c) deposition was accompanied by substitution of the PS skeleton with metal

Preference has been given to this method because it allows to grow highly ordered arrays of vertical pore channels of required geometry, which enables us to easily manage the morphology of further depositing metal films. The control of the PS parameters is realized by variation of electrical regimes of the anodization and concentration of HF in electrolyte as well as by type of conductivity and doping level of the starting Si wafer. Below several parameters of anodization process crucial for PS technology are considered.

Type of starting Si wafers has a determinant influence on the morphology of PS formed by the anodization. During our research work, we were focused on three types of the PS morphology: (1) mesoPS, (2) macroPS and (3) “mixed” PS. To ensure reproducible parameters of *mesoPS* we used the Si wafer of n^+ -type (highly doped with antimony) with resistivity ranging from 0.01 to 0.005 Ohm·cm [8-10, 12-14, 19]. The low resistivity of Si provides no need in an evaporation of a thin metal film on the wafer backside for uniform current flow, which is usually required in the case of a high resistivity. MesoPS based on highly doped Si wafers possesses good thickness and porosity uniformity over the wafer diameter and high reproducibility of the PS parameters from sample to sample. *MacroPS* was formed on p^- -Si (lightly doped with boron) wafers with the resistivity of 10 – 20 Ohm·cm covered in backside with Al film to provide a uniform current distribution [11, 15, 16]. The last type of the PS template presenting combination of meso- and macroPS (so-called “mixed” PS) was grown on p -type Si wafer (boron doped, 0.3 Ohm·cm) [9]. Its conductivity was high enough to exclude backside contact.

Concentration of HF in the electrolyte is the second important factor, which greatly influences the structural parameters of PS. For the anodization of highly doped Si wafers pure aqueous or mixed aqueous-alcoholic solutions of HF are usually used. In case of pure aqueous solutions, a rigorous stirring of the electrolyte is required to ensure the removal of hydrogen bubbles evolved during the dissolution of Si from the PS surface. Otherwise non-uniform PS layers are formed. Aqueous-alcoholic electrolytes are free of this drawback. That is why in our works solution of HF (45 %) : H₂O : C₃H₇OH mixed at the ratio of 1 : 3 : 1 (by volume) was applied [8-10, 12-14, 19]. Anodization of the moderately or lightly doped Si wafers was performed in the solution of HF (45 %) and dimethyl sulfoxide (DMSO) mixed at the ratio of 10 : 48 (by volume) [9, 11, 15, 16].

Current density is the third major technological factor that affects the kinetics of formation and structural parameters of PS. Typically, galvanostatic mode is used if the current is maintained constant by the galvanostat as a current source, thus allowing a thorough control over the PS thickness. For the fabrication of mesoPS in electrolytes containing 10–32 % HF, it is recommended to apply anode current density of 20 – 150 mA/cm² [8-10, 12-14, 19]. To improve the homogeneity of the PS structure throughout the full thickness it is appropriate to use a pulsed mode anodization. It was recently shown that roughness of the pore walls can be significantly reduced if the anodization is carried out in a pulsed mode under a strong magnetic field conditions [4]. To form macroPS and “mixed” PS we have used anodic current density of 8–10 mA/cm² [9, 11, 15, 16].

Fabrication and Morphology of Nanostructured Metal Films onto Porous Silicon

Nanostructured metal films can be formed onto PS by diverse means, which in general are divided in two major groups: (1) dry and (2) wet deposition. The first group includes sputtering, evaporation, atomic layer deposition, chemical vapor deposition, etc. Such techniques are successfully applied for deposition of metal films onto the outer surface of PS, while the methods of the second group result in covering both outer and inner surface of PS due to deep penetration of metal ions in the pore volume from the liquid solution. There are electrochemical, chemical and immersion depositions among the wet methods. In the following section, we consider specific regimes of different deposition techniques used for fabrication of nanostructured metal films onto PS as well as typical morphologies of the obtained structures and the results of their composition and elemental analysis.

Sputtering is an example of the dry deposition methods, which provides precise control of thickness of the depositing metal film in the nanoscale range. Recently we have reported on magnetron sputtering of Nb on mesoPS [10, 14]. Nb was deposited in an UHV dc diode magnetron sputtering system with a base pressure in the low 10⁻⁸ mbar regime. Fig. 3 shows SEM top views of the initial PS and the same sample after Nb sputtering for different periods. The diameter of pores and interpore distance of the PS template were found to vary in the ranges of 10 – 20 and 20 – 50 nm, respectively (Fig. 3, a). It is clearly seen, that Nb was deposited as a nanostructured film consisted of Nb NPs. From Fig. 3, b follows that the growth of the Nb NPs was initiated onto the outer surface of PS. Average NPs' diameter was found to increase simultaneously with the film thickening. For example, Nb NPs in the film of 7.5 nm thickness had diameters about 10 – 15 nm, while in the film of 15 nm thickness they increased up to 20 – 50 nm. In the first case, the Nb NPs were smaller than the interpore distance causing formation of the network of Nb NWs inherited pattern of the outer surface of PS (Fig. 3, b). Further thickening of the Nb film and growth of its NPs promoted their coalescence into continuous film and complete closing of pore entrances, which led to the smoothing of pattern inherited from the underlying PS (Fig. 3, c).

Managing pattern of the outer surface of PS opens an opportunity to form metal films with more clearly defined pattern. This is illustrated in Fig. 4, which shows SEM top views of PS with wider pores before and after sputtering of Pt films. Pt was found to deposit as particles of nanoscale

diameters similar to case of the Nb films sputtering. Despite the thickness of the Pt film was increased greatly, its NPs, in contrast to the previous Nb example, coalesced into the network of wires lying on the outer PS surface. Therefore, the pattern of metal film was not lost due to expanded pore diameters and the clean-cut PS skeleton.

Summarizing, the careful control of the PS morphology and regimes of metal sputtering can result in fabrication of the ultrathin metal films onto PS, which completely inherit pattern of the outer surface of PS as it was presented in schematic illustration in Fig. 2, a.

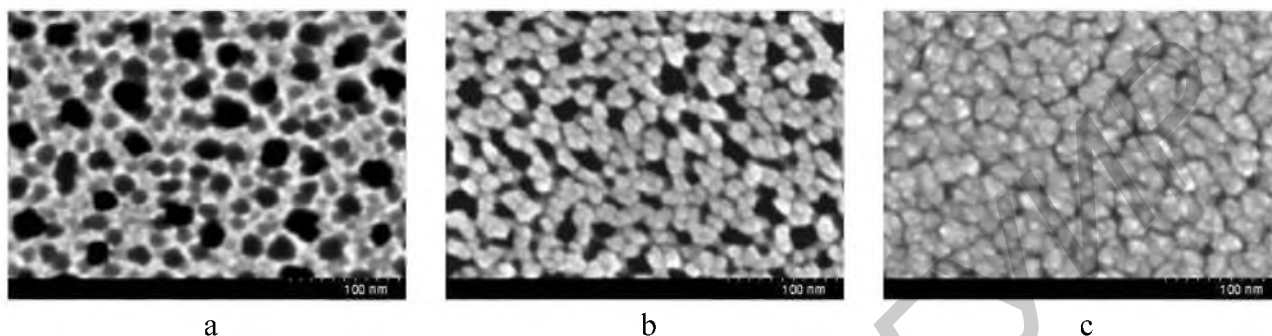


Fig. 3 SEM top views of PS (a) before and (b, c) after magnetron sputtering of the nanostructured Nb films; thickness of the Nb films is (b) 7,5 and (c) 15 nm

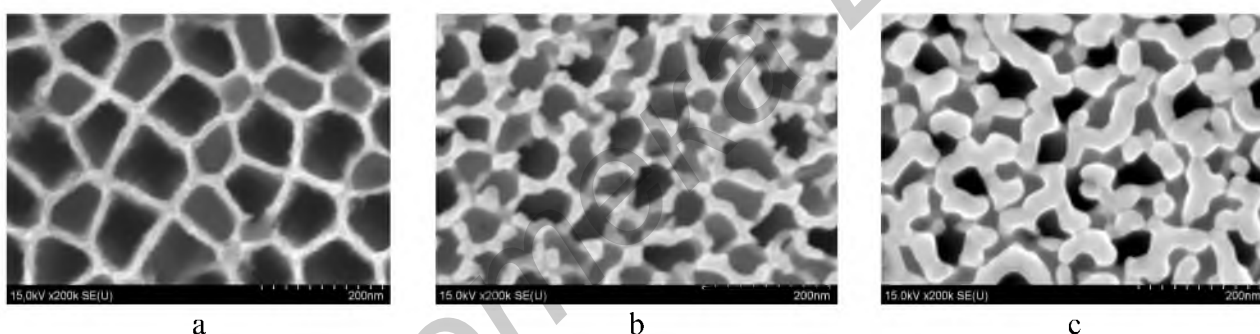


Fig. 4 SEM top views of PS (a) before and (b, c) after magnetron sputtering of the nanostructured Pt films; thickness of the Pt films is (b) 35 and (c) 75 nm

Electrodeposition specifics consists in possibility to fabricate the metal films completely repeating outer and inner surface relief of the porous template. However, in case of mesoPS diffusion limitations in the pores of nanoscale diameter (2 – 50 nm) and weak conductivity of the PS skeleton cause formation of NPs or NWs in the pore channels [2, 4-6]. That is why macroPS is more suitable for covering the PS skeleton with a continuous metal film. In papers [11, 15] the results on electrodeposition of Ni onto macroPS have been presented. Pore diameter and PS thickness altered in the ranges of 500 – 2000 nm and 1 – 12 μm , respectively. Ni was deposited from an aqueous solution of $\text{NiSO}_4 \cdot 7\text{H}_2\text{O}$, $\text{NiCl}_2 \cdot 6\text{H}_2\text{O}$, H_3BO_3 and saccharin mixed at the ratio 213 : 5 : 25 : 3 (in g/l). The solution composition was slightly different from the Watts bath traditionally used for Ni electrodeposition [4]. Current density of 10 mA/cm^2 was applied for different periods depending on the required Ni film thickness. Fig. 5 shows SEM images of macroPS of 2.5 μm average thickness, which was used as a template for the Ni deposition in [15]. Cylindrical pores with rounded bottom perpendicularly oriented to the sample plane are typical for macroPS. The pore length of macroPS can be increased up to the Si wafer thickness. In our works [11, 15, 21] we used macroPS with 1 – 15 μm pore length.

After Ni electrodeposition the structure and composition of the samples were studied by XRD and SEM analysis. It was found, that deposited Ni has a polycrystalline nature with (111), (100) and (110) dominated crystalline orientations.

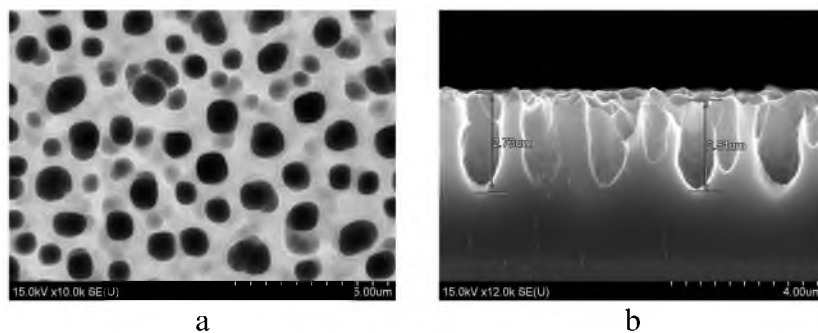


Fig. 5 SEM (a) top and (b) cross sectional views of macroPS

Fig. 6 shows SEM images of macroPS after electrodeposition of Ni for 4 min. It is observed, that Ni deposits on the outer and inner surface of macroPS as the continuous film of uniform thickness about 300 nm. Electrodeposition prolonged to 10 min leads to the pores closing due to thickening of the Ni film.

The structure of the Ni films in thicker macroPS (5 – 12 μm) was hidden in the SEM images because of non-perpendicular cross-sections and large pore length. Thus, it was difficult to find if the Ni film completely covers the inner surface of PS. We performed an additional treatment of the experimental samples to reveal the structure of Ni films in depth of the PS template [15]. MacroPS samples with the thickness of 5 – 12 μm covered with Ni film were immersed in the solution of $\text{H}_3\text{PO}_4 : \text{HNO}_3 : \text{CH}_3\text{COOH} : \text{H}_2\text{O} = 2 : 2 : 7 : 5$ (vol. ratio) at 30 °C. The immersion was stopped just after full etching of the Ni film from the outer surface of PS. At the same time, Ni film on the inner surface of PS was not removed yet. Then the macroPS skeleton was removed in KOH solution at 60 °C. As a result, the rests of Ni film deposited onto the inner surface of PS were opened. Fig. 7 shows SEM images of the revealed Ni films, which were formed by electrodeposition. Analysis of the images left no doubts that Ni film completely covered the pores up to their bottom forming void-like structures. Moreover, it was found that Ni films had uniform thickness along on the whole surface of macroPS.

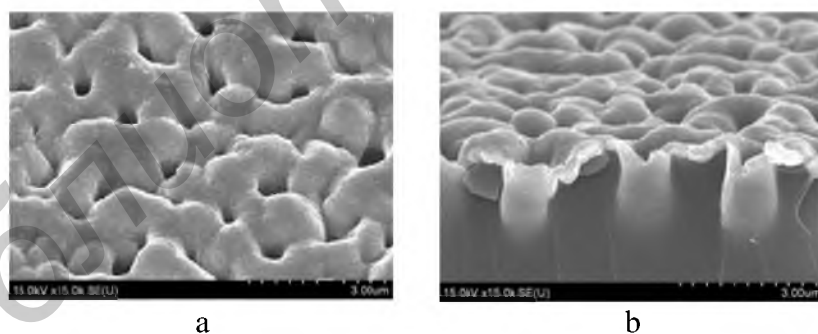


Fig. 6 SEM (a) top and (b) cross sectional views of macroPS after Ni electrodeposition

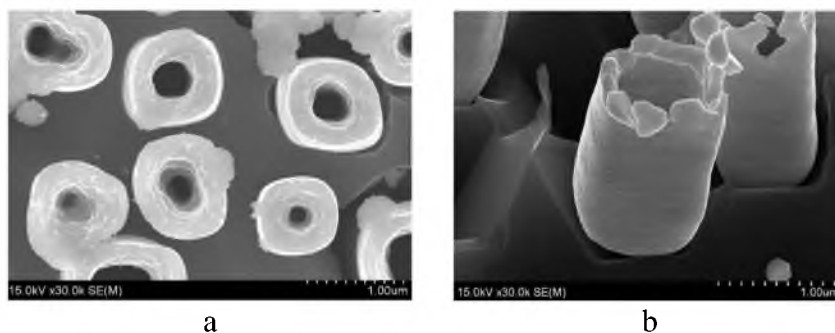


Fig. 7 SEM (a) top and (b) cross sectional views of Ni films formed onto the inner surface of macroPS by electrodeposition

The obtained results have shown that using macroPS as a template for metal electrodeposition one can fabricate the continuous metal films with uniform thickness both onto the outer and inner surface of PS. Ni films repeating the specific relief of macroPS can be considered as arrays of so-called metal nanovoids schematically illustrated in Fig. 2, b.

Immersion deposition occupies a special place among wet metal deposition techniques since this method allows to form metal films on the substrate without applying an external potential or reducing agents in solution in contrast to electrodeposition or chemical depositions. Immersion deposition of metal atoms on a substrate is carried out due to redox reactions between atoms of substrate material and metal ions from the solution. In case of Si-based substrates, solutions containing ions of metal with positive redox potential (Cu, noble metals) have to be used to perform immersion deposition. Our research group has studied immersion deposition of different metals onto PS for more than one decade [2, 8, 9, 12, 13, 16, 21-24]. The mechanism of the process and properties of fabricated materials have been revealed. An extremely important result is development of the immersion deposition model depending on the type of the initial Si wafer, the PS morphology and conditions of the metal deposition including time and temperature regimes and solution composition. It has been found, that proper combination of these factors can lead to the partial or complete substitution of Si atoms in the PS skeleton with metal atoms causing fabrication of all types of the nanostructured metal films illustrated in the introduction section of this review. Here we consider the most recent results on fabrication of the nanostructured metal films onto PS by immersion deposition.

Ag immersion deposition. In paper [16] immersion deposition of Ag on macroPS was performed. The structure of macroPS was the same presented to that in Fig. 5 in the previous subsection. Fig. 8 demonstrates SEM images of macroPS after immersion for 40 min into the bath composed of the 3 mM AgNO₃ aqueous solution, HF (45%) and C₂H₅OH mixed in the volume ratio 20 : 1 : 2. XRD analysis of PS after immersion into the solution for Ag deposition showed a polycrystalline nature of the Ag deposit. From Fig. 8 follows that Ag deposited only on the outer surface of macroPS as a film consisted of Ag dendrites. Each dendrite was a slightly branched “tree” grown from Ag NPs and nanosheets of 20 – 100 and 150 – 600 nm in diameter. It was found, that Ag dendrites formation was possible due to covering the outer surface of PS with the Ag NPs which acted as precursors and saturation of the solution with the Ag ions. At the same time, concentration of electrons for the Ag ions reduction was low enough because of *p*-type of the initial Si wafer. Absence of the Ag deposit on the inner surface of PS is caused by its relative smoothness and wettability of the solution improved by addition of isopropanol, which provided slipping Ag NPs along the pore walls to the outer surface and their further integration with the Ag dendritic film. Dendrites in the Ag film were observed to be ordered in accordance to the pattern of the outer surface of PS.

Cu immersion deposition. Remarkable morphology was observed in nanostructured Cu films formed by complete substitution of the PS skeleton with Cu atoms during immersion deposition [13, 24]. Fabrication of such film was realized due to the use of “mixed” PS as a template for deposition of Cu.

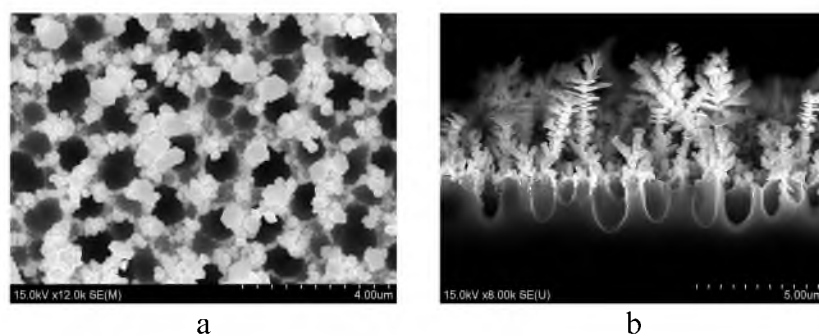


Fig. 8 SEM (a) top and (b) cross sectional views of the nanostructured Ag films formed onto the outer surface of macroPS by immersion deposition

SEM images of the “mixed” PS are presented in Fig. 9. Its morphological type can be defined as a mixture of macro- and mesoPS, because there can be observed major macropore channels perpendicular to the substrate plane, while basing macroPS skeleton is riddled with mesopores (especially in the top part). The average thickness of the “mixed” PS was about 3 μm . Such morphology of PS is favorable for deep penetration of the solution to the inner surface of PS due to the presence of the macropores. Furthermore, reduced dimensions of the “mixed” PS skeleton provided by riddling with mesopores made their dissolution at the Cu deposition faster and easier. An important condition for the substitution of Si atoms with Cu ones is *p*-type of the initial Si wafer. In the case of *n*-type, reduction of Cu ions is carried out mostly due to electrons of the dopants preventing oxidation and dissolution of the PS skeleton [25, 26].

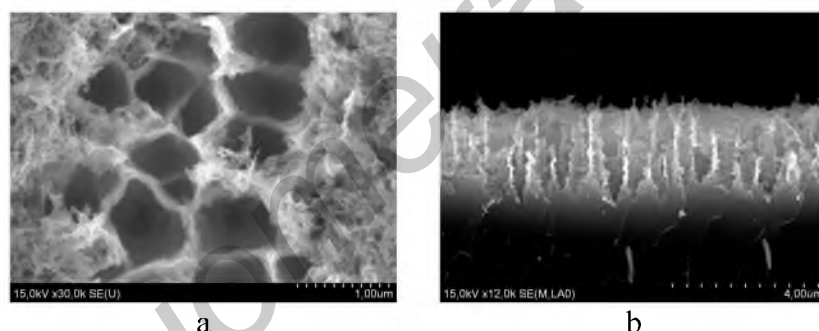


Fig. 9 SEM (a) top and (b) cross sectional views of the “mixed” PS

Deposition of Cu was performed by immersion of the “mixed” PS in 0.025 M $\text{CuSO}_4 \cdot 5\text{H}_2\text{O}$ + 0.005 M HF (45%) + 0.1 M $\text{C}_3\text{H}_7\text{OH}$ aqueous solution for 30 – 120 min. Upon reaching immersion time 120 min, deposited Cu film was separated from the substrate opening surface of the initial Si wafer free of the PS rests. It was an evidence of the complete dissolution of the PS skeleton. XRD and EDX analysis showed that the separated film contained about 99 at. % of Cu and had polycrystalline nature. Fig. 10 demonstrates SEM images of cross section, top and bottom views of such Cu film. It is observed that the film was porous and consisted of two layers. Its average thickness was about 8 μm . The top view shows the surface of the sample/solution interface, while the bottom – surface initially connected with the substrate. The top layer had the thickness of about 5 μm and presented a tightly packed array of parallel column-like agglomerates, which were perpendicular to the substrate plane, i.e., columns grew along the pore direction of the original PS. On the other hand, the bottom layer looks like a sponge of 3 μm in thickness consisted of chains of the Cu particles. The diameters of upper agglomerates are an order of magnitude greater, than those of bottom particles. In the spongy layer, the particles of 100 to 200 nm in diameter dominated. The diameter range of the upper agglomerates was 1500 to 3500 nm. The gravimetrically determined porosity of the Cu film was 60 – 65 % in comparison with bulk Cu and equaled to porosity of the initial “mixed” PS.

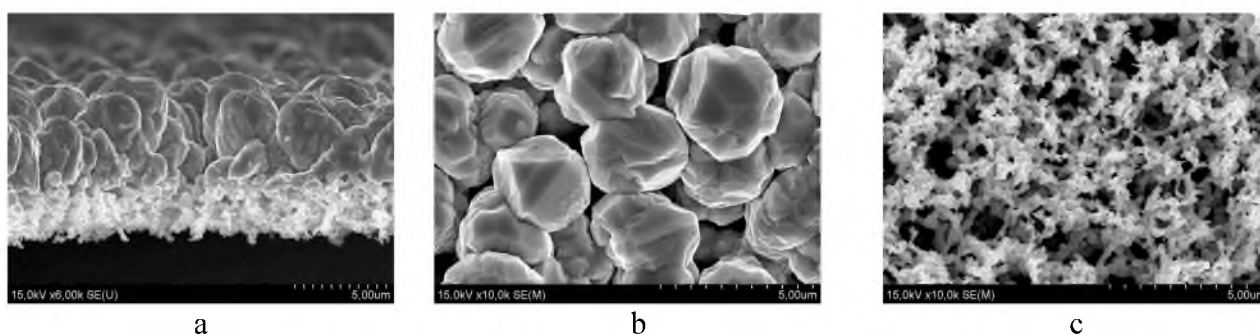


Fig. 10 SEM (a) cross sectional, (b) top and (c) bottom views of the nanostructured Cu film formed by immersion deposition of Cu onto “mixed” PS

The formation of the nanostructured Cu film was found to proceed as follows. At the stage of full impregnation of PS with the solution, Cu NPs nucleate and grow on the surface of PS skeleton. Since metal reduction is carried out simultaneously with dissolution of Si, the PS skeleton was substituted with the bottom spongy Cu layer. It is proved by the equality of the thickness of the original PS to that of the bottom Cu layer (3 μm). After that, new Cu NPs grow and coalesce onto the outer surface of the spongy Cu layer. In this way, the layer of huge Cu agglomerates is formed. Cu film is separated in the moment when stresses on the Si substrate/Cu film interface exceed the interaction force between Si and Cu atoms.

Summarizing, immersion deposition of metals onto PS allows to fabricate a number of different morphological types of nanostructured metal films inheriting the structural peculiarities of the original PS template as it is schematically shown in Fig. 2, a and c.

Combination of different deposition techniques and metals is very attractive for fabrication of nanostructured multi metal films onto PS, i.e. films composed of several metals. Such approach can significantly enhance or change properties typical for the single metal film. Here we present our recent results on forming nanostructured bimetal film onto macroPS by successive Ni electro- and Ag immersion depositions [15]. MacroPS showed in Fig. 5 was used as an initial template. Ni electrodeposition was carried out upon the conditions described in the subsection on electrodeposition. However, Ni deposition time was no longer than 2.5 min to avoid pore closing. After plating macroPS with Ni film, the sample was immersed into aqueous solution of 3 mM AgNO_3 , HF (45%) and $\text{C}_2\text{H}_5\text{OH}$ mixed in the volume ratio 20 : 1 : 2 for 30 min. Fig. 11 presents SEM images of the resulting sample. It is observed that the outer surface of the Ni film is covered with tightly packed spherical Ag nanoparticles which diameters alter from 10 to 150 nm. Cross sectional view shows that Ni film on the inner surface of macroPS was partially dissolved to sponge-like layer due to Ag immersion deposition. According to EDX analysis the sample contained 35 at. % of Ni and 2 at. % of Ag.

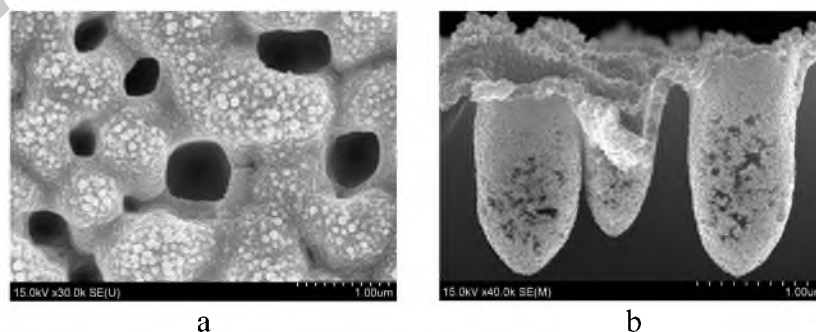


Fig. 11 SEM top and cross sectional views of nanostructured bimetal (Ni-Ag) film formed by successive Ni electrodeposition and Ag immersion deposition onto macroPS

Schematic view of the obtained nanostructured bimetal film on PS is illustrated in Fig. 2, c and presents an array of bimetal nanovoids.

Properties and Applications of Nanostructured Metal Films onto Porous Silicon

Arrays of Superconductive Nanostructures. Research activity in the field of superconductivity at reduced dimension has been continuously growing [28, 29] because its results can help to understand fundamental aspects of this phenomenon resulting in practical application in superconducting electronics [29-31]. The behavior of superconducting nanostructures of dimensions comparable with the superconducting coherence length is dominated by both thermal activated phase slips (TAPS) and quantum phase slips (QPS) processes [32] causing the nanostructures to remain resistive much below the superconducting transition temperature. The challenge of the experimental study of such nanostructures is the problem of fabrication of homogeneous samples, since it has been widely demonstrated that sample inhomogeneity can be the source of broadened superconducting transitions [33]. From the early studies realized on crystalline superconducting whiskers, advances in nanofabrication techniques have allowed the realization of high quality single crystals nanowires [34, 35]. Even more sophisticated is the approach of using suspended carbon nanotubes or DNA molecules as templates for the formation of superconducting nanowires [36-38]. A radically different approach to nanostructures fabrication based on self-assembled growth attracted much attention also in the superconducting nanowire field [39, 40]. Most of these works rely on the deposition within the channels and cavities of porous membranes. Self-assembled methods are versatile and reliable bottom-up techniques for generating low-cost patterns of nanostructures, assuring a highly reproducible geometry on very large areas. We have proposed to study superconductivity of the interconnected Nb nanostructures in the film deposited onto mesoPS by magnetron sputtering [10, 14]. Typical morphology of the nanostructured Nb films formed for the research is presented in Fig. 3, b. Analysis of SEM images showed that average size of the Nb nanostructures is comparable to the superconducting coherence length. Hence, each individual Nb nanostructure behaves as a one dimensional (1D) object. As a consequence, the whole samples show broadened resistive transitions, which can be described by theoretical models for both thermal and quantum fluctuations of the order parameter in 1D superconductors [41, 42]. Since the effect of the periodic PS template is reduced if the Nb film thickness exceeds the pore diameter, Nb films deposited for transport measurements were no thicker than 12 nm. Moreover, the thickness of the Nb film optimal to investigate superconducting properties of the Nb nanostructures was found to fall in the range from 9 to 12 nm. To perform resistivity measurements, the samples of Nb films on mesoPS were patterned by standard optical lithography and lift-off procedure into stripes of 10 – 20 nm in width and 100 μm in length. In this way four-point geometry of Nb film (meaning two contacts, each used to set/register current and potential) was realized. The goal of the patterning was to reduce the number of interconnected Nb nanostructures upon measurements. Superconducting transition temperatures and critical currents were resistively measured in a Helium cryostat using a standard dc four-probe technique. Transport measurements were also provided to control quality and homogeneity of the Nb nanostructures. Fig. 12 shows the resistive transitions for all the analyzed samples. Measurements were performed using a constant bias current 50 μA . The first step in the curves is due to the transition of the electrodes [27, 36]. The main feature of the R(T) curves is the nonzero resistance over a wide temperature range, which is strongly reminding a 1D behavior. It also deserves noticing that the R(T) curves do not show any steps or humps, which can be a signature of inhomogeneity [33].

The proposed technique allows one to overcome the problem of handling fragile membranes usually used for this purpose [39, 40] employing robust PS crystals as a stable support. Moreover, the analyzed systems are rather simple and macroscopically large objects, which however, reveal fascinating quantum effects. Finally, compared to similar self-assembled nanowire networks exhibiting thermal phase slippage [40], the system presented in this work provides strong evidence of QPS.

SERS-active substrates. Raman spectroscopy is an important analytical method for chemical and biological analyses due to high structural information content. However, applicability of this technique was restricted for many years because of an extremely small Raman scattering (RS) cross section, thus preventing the possibility of low concentration detection. The renewed interest in Raman spectroscopy has been emerged due to the observations of enormous enhancement of Raman signal for molecules adsorbed on special metal surfaces with nanoscale roughness [43-45]. This so-called surface-enhanced Raman scattering (SERS) phenomenon opens a wide range of new possibilities of the Raman technique for trace chemical analyses, environmental monitoring and biomedical applications [46-49].

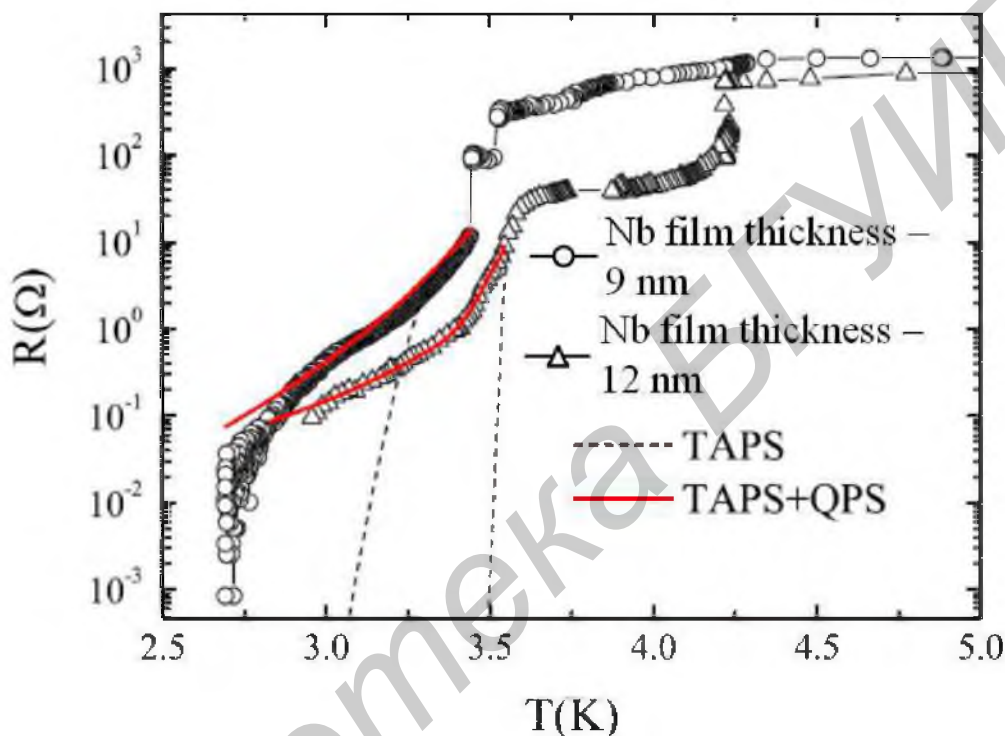


Fig. 12. Resistive transitions of different nanostructured Nb films: experimental data of the Nb films with thickness 9 nm (circles) and 12 nm (triangles) are shown together with the curves obtained from theoretical calculations including only the TAPS term (dashed black lines) and both TAPS and QPS terms (solid red lines).

Moreover, under special conditions, enhancement factors of about 14 orders of magnitude, as compared with conventional non-resonant RS, can be achieved [50]. The large Raman cross section permits single-molecule detection [51, 52]. SERS-activity is known to be demonstrated by metal nanostructures. An electromagnetic field of the metal nanostructures increases under laser excitation at the Raman scattering due to an effect of surface plasmon resonance (SPR). Fabrication of the films consisted of metal nanostructures allows to improve SERS-activity because of multiplication of the electromagnetic field in the closest locations of metal nanostructures (so-called “hot spots”). Despite all metals show SPR, noble metals are mostly used in SERS-active substrates as they are characterized by SPR in the visible range and demonstrate high stability. Thus, the most critical aspect of SERS is the development of new noble metal substrates. The substrates need not only to have a rough nanoscale features, but also should demonstrate high sensitivity, reproducibility, stability, ease of preparation and compact size. Traditional SERS-active substrates include electrodes roughened by the oxidation–reduction cycle and aggregated colloidal NPs. Rough metal electrodes are stable and reproducible, but they have low sensitivity and unhandy for many applications. On the other hand, aggregated colloids can be easily prepared and often provide the strong Raman enhancement, however such substrates are typically unstable and difficult to reproduce. Many new SERS-active materials have been appeared during the last decade due to

progress in nanotechnologies. The growing interest to the nanofabrication is obvious since SERS enhancement depends on the size, shape, and interspacing of noble-metal NPs [53]. There are several methods for the formation of such surface-confined nanostructures, including electron-beam lithography [54], nanosphere lithography [55], and films over nanospheres [56]. However, practically all these materials are costly, require special technique and trained personals for the fabrication. It has been shown that PS appears to be promising material for the fabrication of SERS-active substrates [57-59]. Our research group has been among pioneers in the area of SERS-active substrates based on PS [8, 60, 61]. The rich family of morphological types of PS allows to fabricate onto its surface different nanostructures demonstrating SERS-activity, which are adopted to careful analysis of a specific molecule or can be used for the study of complex analytes. For instance, we have applied as analytes a number of organic and inorganic objects, including heavy metals, graphene, carbon nanotubes, organic dyes, porphyrines, proteins, etc. Principal attention to SERS of metal porphyrines in some of our works is caused by prospects of porphyrines in therapy of cancer, anemia, neuropsychiatric disorders, skin and eye diseases. Functions of the molecular porphyrine systems used for selective treatment are based on their interaction with different biomolecules (mostly with transport proteins and nucleic acids). Proper therapy has to provide immediate and invasive detection of porphyrine at extremely low concentration in physiological liquids of patient. So, SERS-analysis fully meets these requirements.

SERS-active substrates based on Ag dendrites on PS. Improved SERS-activity can be possessed by Ag nanostructures, especially dendritic films, due to many crossing tips of Ag nanostructures favorable for “hot spots”. As it was described above, one way to form such films is Ag immersion deposition on macroPS. Actually, driving force for the study of Ag dendrites growth on macroPS was our previous result on SERS-activity of immersion deposition of nanostructured Ag film on mesoPS [12, 25]. The Ag immersion deposition on the mesoPS based on n-Si has led to the forming the Ag NPs on its outer surface. The growth of the Ag dendrites has not been observed due to the excess of electrons from the substrate for the Ag reduction. In the work [16] the overabundant number of the electrons from the dopant atoms was avoided by using the macroPS formed on the p-Si wafer. Reflectance spectrum of the Ag dendritic film on macroPS showed that the the position of its SPR band is located between 370 and 500 nm with the maximum absorbance around 450 nm. The best condition for the SERS spectra registration is using the laser wavelength within the SPR range of SERS-active substrate. Thus, we applied blue laser of 473 nm wavelength. The laser power density was 0.8 kW/cm². Fig. 13 presents SERS-spectra of water-soluble cationic Cu(II)-tetrakis(4-N-methylpyridyl) porphyrin (CuTMpyP4) adsorbed on the dendritic Ag film deposited on macroPS for 80 min. The spectra contain all bands typical for Raman spectrum of this compound. The study of the analyte on the macroPS free of Ag showed just background proving evidence of SERS-activity of the dendritic Ag film. Following from Fig. 13 detection limit of SERS-active substrate based on Ag dendrites on macroPS reached 10⁻¹⁰ M, while minimal concentration of the porphyrine detected by ordinary Raman spectroscopy did not exceed 10⁻⁴ M.

SERS-active substrates based on metal nanovoids on PS. SERS-active substrates based on films composed of NPs of different shapes (spheres, triangles, rods, etc.) are defined in the literature as 2D nanostructures. However, recently principally novel 3D SERS-active nanostructures have attracted a great attention of the scientific community [62]. It has been found that arrays of metal nanovoids (anti-NPs) demonstrates significant SERS-activity. Surface plasmons in this case are localized within and around nanovoids in metal film. Fabrication of nanovoids is quite easy and includes convective assembly [63, 64] or vertical deposition [65] of polymer nanospheres on a base support (metal coated glass) followed by electrodeposition of metal. Finally, polymer is removed leaving a metallic film with the highly ordered array of voids. Such technique provides remarkable reproducibility and repeatability of the properties of SERS-active substrates. Easy control of the

thickness of deposited metal by monitoring the current density as well as possibility of successive deposition of different metals allows variation of the nanovoids parameters in a very wide range. These factors make nanovoids substrates perfect for studying SERS phenomena.

Nevertheless, the area of monolayer of polymer spheres on the base support is usually limited (about 1 cm^2) because exceeding such sizes prevents self-organization of spheres and causes defects in the layer. In this regard, it is very prospective to develop a method of nanovoids production excluding the polymer spheres coating. We proposed fabrication of SERS-active substrates based on nanovoids by direct metal deposition from solutions on macroPS. To improve the SERS-activity we have used bimetalization consisted of Ni and Ag. Ni was chosen as transition metal to expand SPR band of SERS-active film [66]. At the same time Ag is known for its strongest plasmonic properties. Our idea was to fabricate basic continuous Ni layer on the pore walls of PS and improve its plasmonic properties by immersion deposition of Ag NPs. The fabrication steps and typical morphology of the resulting bimetal films were presented in the previous sections. The reflectance spectrum of the bimetal film on macroPS showed that the position of its SPR band is located between 300 and 500 nm. Maximum absorbance peak was not as sharp as for dendritic Ag film and laid in the range 410 – 470 nm.

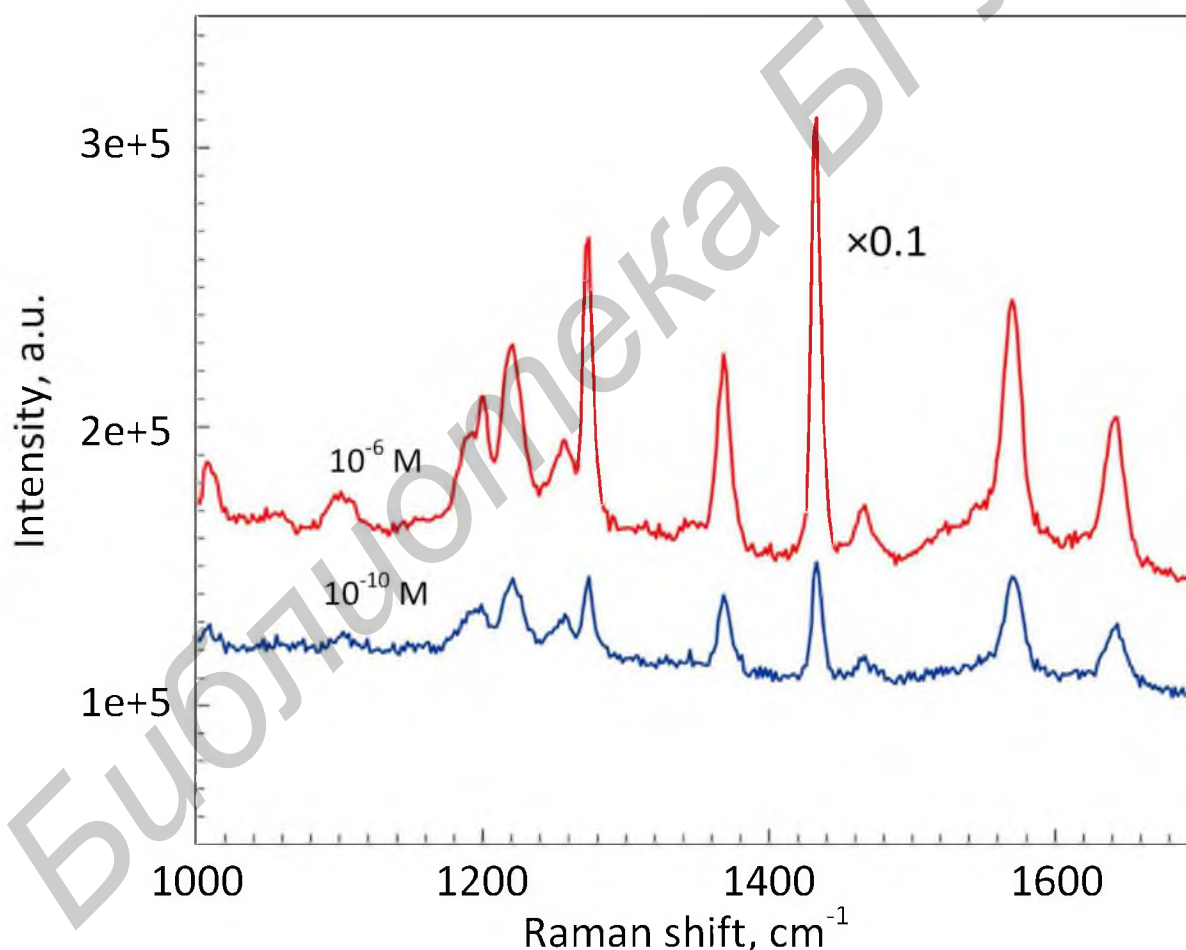


Fig. 13. SERS spectra of CuTMpyP4 molecules adsorbed on the dendritic Ag film grown onto the macroPS by immersion deposition for 80 min

Broadening of the SPR was caused by Ni contribution. Thus, addition of transition metal gives an opportunity to vary SPR in the wide range. The best condition for the SERS-spectra registration is using the laser wavelength falling within the SPR range of SERS-active substrate. SERS spectra were recorded by using Solar TII DM160-MS3504I spectrometer with excitation at 441.6 and 514.5 nm by He-Cd and Ar ion lasers respectively. The power density of lasers was about 0.3 – 0.5

W/cm². Fig. 14 shows SERS spectra of CuTMpyP4 adsorbed on the nanostructured bimetal film formed by consecutive Ni electrodeposition and Ag immersion deposition on macroPS.

Raman signal enhancement was estimated on the intensity of the band at 1365 cm⁻¹ (marked by dashed line in Fig. 14). The highest signal is observed for the substrate formed by immersion deposition of Ag for 30 min. SERS signal intensity reaches 10⁵, in contrast to 10⁴ for two others substrates. The morphology of this sample was shown in Fig. 11. Significant signal enhancement is partially caused by optimal dimensions of Ag NPs (10 – 150 nm) which are favorable for SPR and thus for SERS effect. In addition, spongy structure of bimetal film on the inner surface of PS provides a number of “hot spots” where abnormally high electromagnetic field is excited. As it was mentioned above, effective enhancement of the Raman signal occurs for the molecules located near “hot spots”. The detection limit of the most SERS-effective bimetal film was studied for the rhodamine 6G (R6G). Laser wavelength of 514.5 nm was used to provide resonant conditions for the plasmons and R6G excitation. Fig. 15 presents SERS spectra for R6G adsorbed on the bimetal film on macroPS from solutions of the altered concentrations. It is observed, that the decrease of the R6G concentration is accompanied by SERS intensity gradual falling. However, 1362 and 1508 cm⁻¹ bands typical for R6G can be observed in all spectra. It follows from Fig. 15 that the detection limit provided by the SERS-active substrate based on the nanostructured Ni-Ag film on macroPS is as small as 10⁻¹¹ M.

Very recently, the developed SERS-substrates have been successfully used to determine concentrations of antiseptic proteins in tear liquids to perform proper treatment of eye diseases [67].

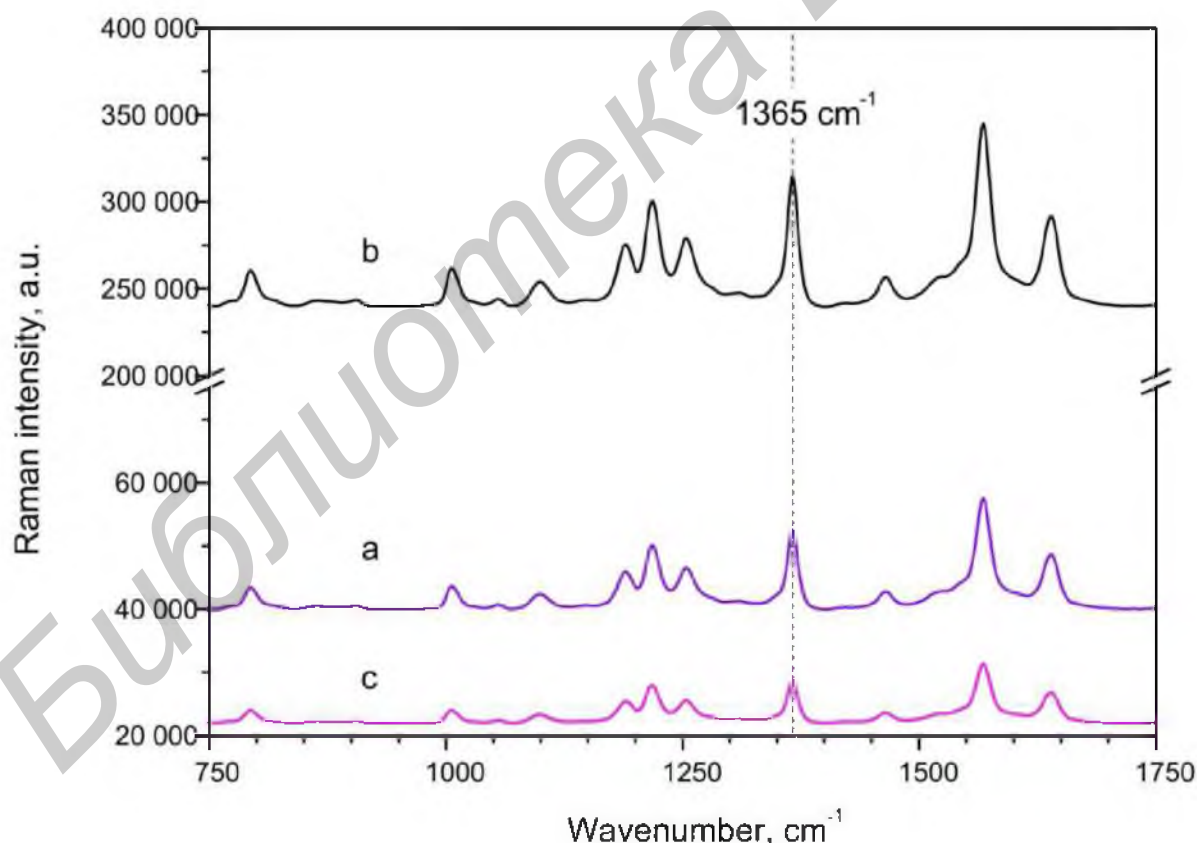


Fig. 14. SERS-spectra of CuTMpyP4 adsorbed from 10⁻⁶ M water solution on nanostructured Ni-Ag film; films was formed by Ni electrodeposition on macroPS for 2.5 min and followed by Ag immersion deposition for (a) 5, (b) 30 and (c) 120 min.

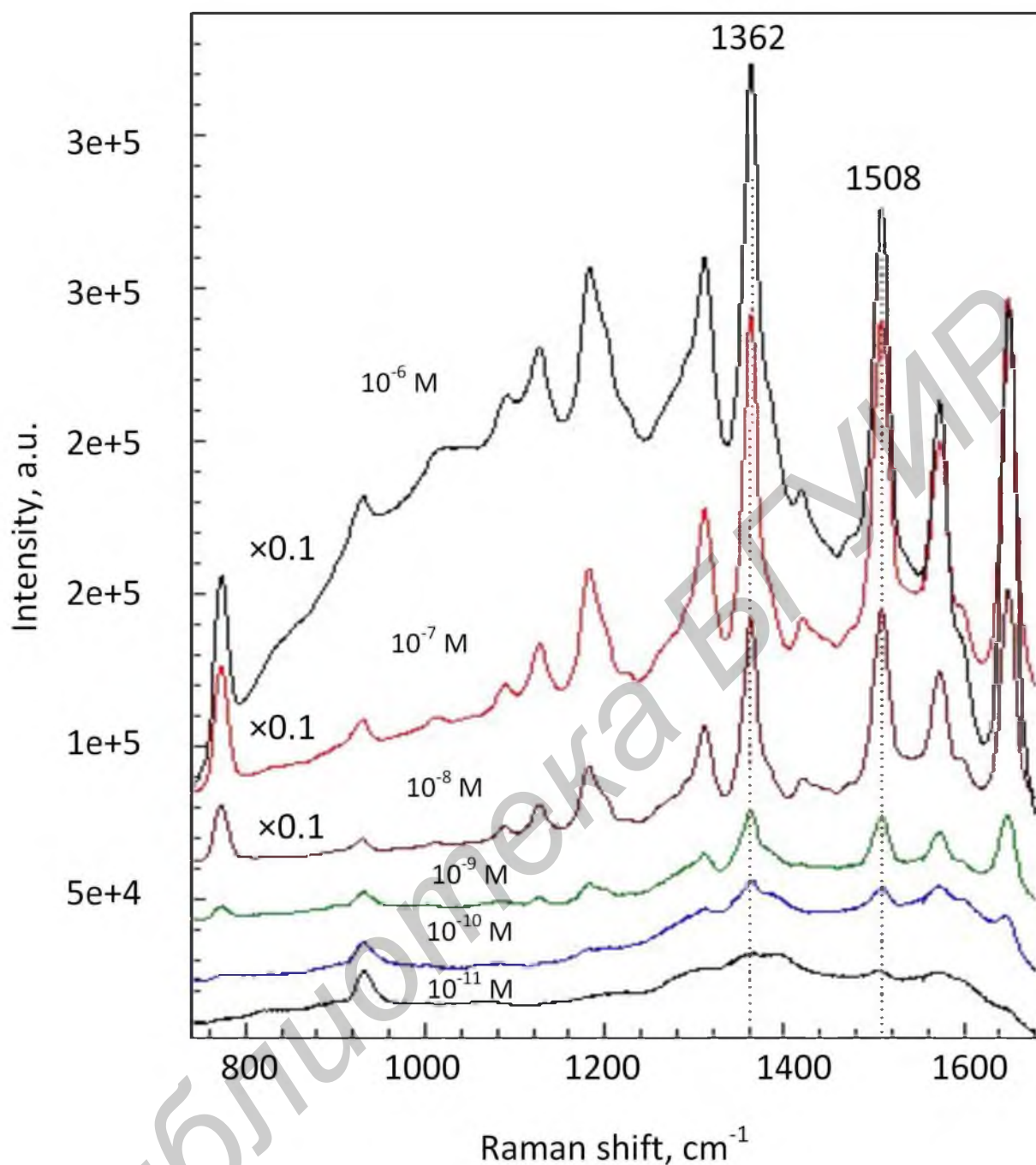


Fig. 15. SERS-spectra of R6G adsorbed on nanostructured Ag/Ni film onto macroPS from the solutions of different concentrations

Elastic Electrodes for transdermal therapy. One of the most important tasks of modern biomedicine is treatment of living tissue pathologies. For the last decade, transdermal drug delivery by electroporation (aquaphoresis, non-invasive mesotherapy, needle-free mesotherapy, no injection mesotherapy) has been considered to solve this problem. The electroporation method provides to introduce macromolecules of active substances, drugs and genetic materials from solutions into living cells by applying short pulses of voltage, which open pores in cell membranes [68]. Effective transdermal delivery by electroporation therapy requires realizing close electrode contact with the vastest possible area of the diseased tissue, i.e. skin. Currently rigid Al electrodes are used for the electroporation. It limits the surface area of the treated tissue resulting in weak healing quality. Development of elastic electrodes could help to overcome this limitation. Such electrodes have to be thin enough for elasticity (several decades of microns) and have porous structure (pore diameters

of nanoscale range). The porosity is caused by need of similarity to living tissues, which are porous in nature for proper organism functionality. Taking into account these requirements, we have proposed nanostructured Cu films formed by substitution of “mixed” PS skeleton as a candidate for material of electroporation electrodes. Cu films are of principal attention due to high conductivity and antibacterial activity of Cu.

Mechanical properties of Cu films based on PS. Elasticity of the nanostructured Cu films was studied by measuring their Young modulus upon temperature variations from -100 to $+100$ °C. We performed the control of Young modulus at different temperatures to reveal the reliability of electrode under voltage pulses, which causes Cu film heating. We used the samples of the free nanostructured Cu film with the thickness of $25\ \mu\text{m}$. Schematic illustration of the measuring process is presented in Fig. 16. Young modulus was estimates in the Cu film plane (E_{\parallel}) and cross section (E_{\perp}).

Fig. 17 shows the temperature dependences of the measured Young modulus. Both E_{\parallel} and E_{\perp} increase at temperature falling. This behavior is typical for the most solid materials. The measured values of Young modulus are significantly lower than that of bulk Cu ($110\ \text{MPa}$). Young modulus in the film plane and cross section varies in the ranges $450 - 900\ \text{MPa}$ and $0.5 - 4.5\ \text{MPa}$ respectively. The decrease of Young modulus of the Cu film in comparison with that of bulk Cu is caused by film nanostructuring. E_{\parallel} is two orders of magnitude higher than E_{\perp} , i.e. mechanic properties of the film are anisotropic. It is connected with peculiarities of the Cu film morphology. Upper Cu layer consisted of agglomerates lays on the layer of the network of Cu particles (Fig. 10). Cu agglomerates are mutually separated causing an easy deformation of the film in its cross section. On the other hand, bottom Cu particles are connected in the network preventing destruction of Cu film. Hysteresis of the Young modulus observed in the curves takes place due to gas adsorption/desorption by porous Cu structure under temperature altering. Variations of Young modulus at $20 - 30$ °C (comfortable temperature for the human skin) do not exceed 20 %.

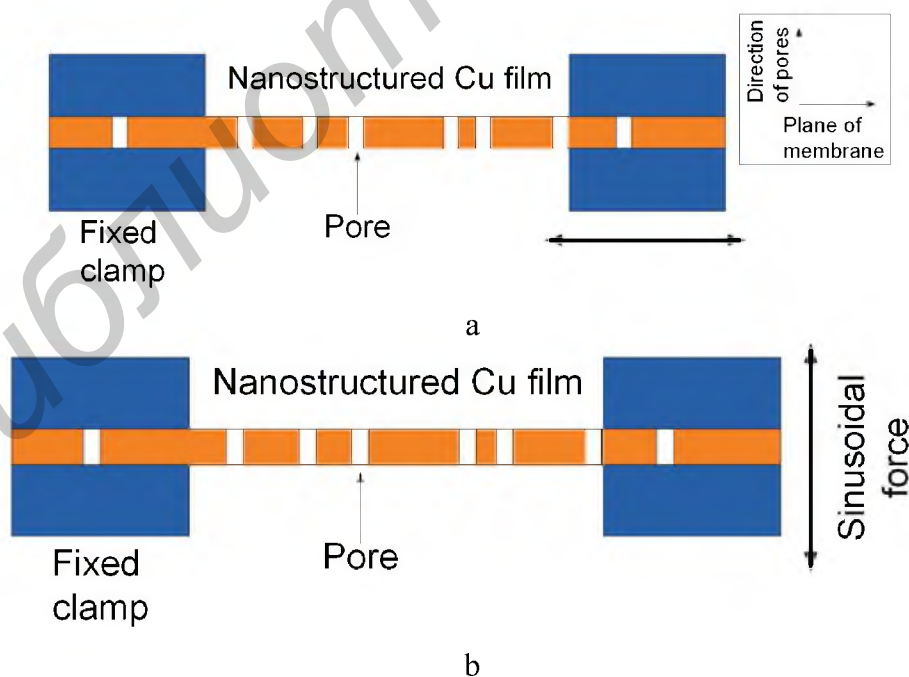


Fig. 16. Schematic illustration of the Young modulus measurements for the free nanostructured Cu film

Electrical properties of Cu films based on PS. Specific electrical resistance of the nanostructured Cu film was measured using samples of 10 , 20 , 50 and $100\ \mu\text{m}$ thickness. Each

sample of Cu film was cut onto 2×20 mm stripes. Then we fixed two conductive probes onto the Cu stripe thus providing press contact. The measurements for each stripe were performed twice: in probe contact with upper and bottom layer. The potential on the strip was measured at current of 100 mA. Using data of the measurements, we calculated values of the specific resistance, which was independent on Cu film thickness. Despite the morphology of the Cu film is not homogeneous (two-layered), its specific resistance was found to be quite uniform. An average specific resistance of the nanostructured Cu films was found to be equal to $2.65 \cdot 10^{-8}$ Ohm·m. Deviations from this value did not exceed $0.05 \cdot 10^{-8}$ Ohm·m proving repeatability of the electrical properties of the Cu film across the single sample and from sample to sample. The specific resistance of Cu film is almost similar to that of bulk Al prevalently used as a material for the electroporation electrodes.

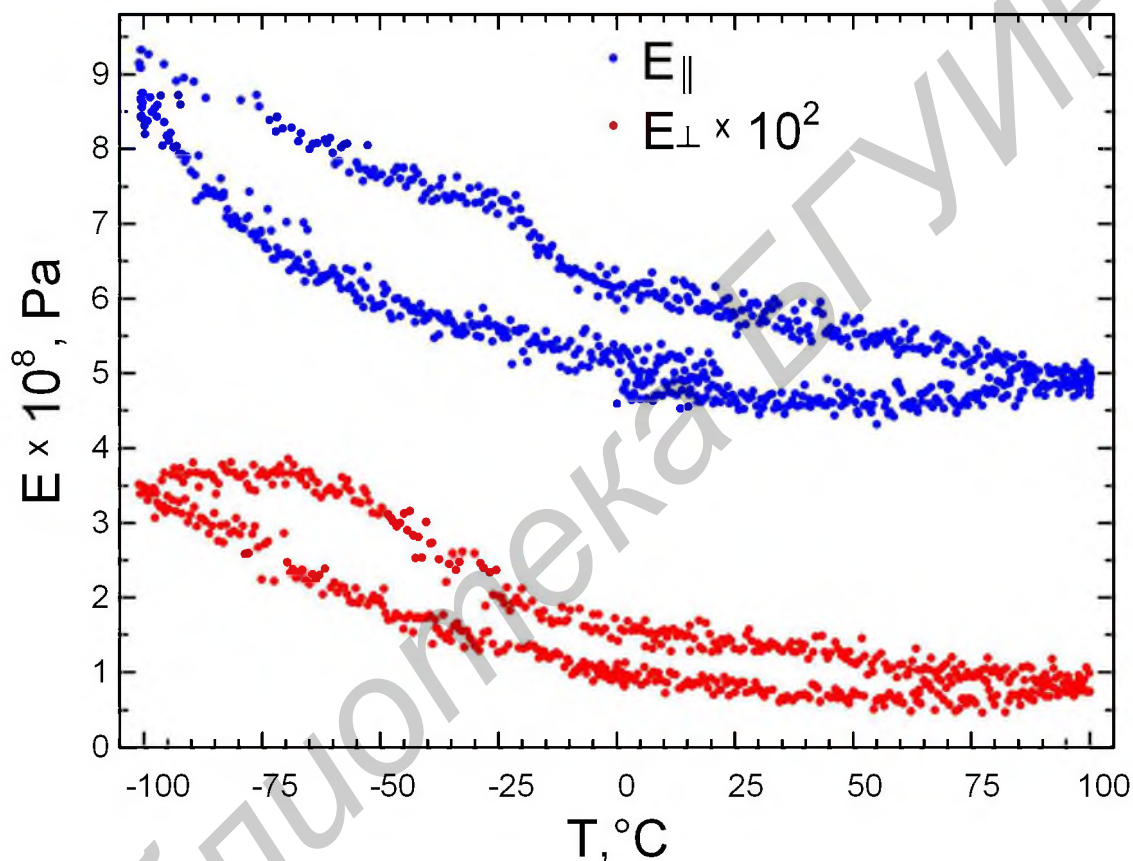


Fig. 17. Temperature dependences of the Young modulus of the free nanostructured Cu film

Therefore, the nanostructured Cu film formed by substitution of “mixed” PS skeleton with Cu possesses properties convenient for its application as a material of the elastic electrode for electroporation.

The obtained results were used to design construction and produce testing sample of the elastic electrode for electroporation of the 50 cm^2 active area [69].

Summary

For more than a decade many efforts have been devoted to the fabrication of the nanostructured metal films onto PS by combinations of different porous templates and metal deposition methods. Impressive morphological types of the metal films have been achieved, including (1) ultrathin metal films onto PS which completely inherit pattern of the outer surface of PS, (2) metal and bimetal films with uniform thickness both onto the outer and inner surface of PS and (3) porous metal films formed by substitution of the PS skeleton with metal. It has been shown that nanostructuring of the

metal films with PS template provides pronounced changes of their properties in contrast to bulk metals. Varied potential applications have been explored for the developed metal films in such areas as superconductive electronics, chemical and biomedical sensing and drug delivery. Although, we can expect further research activity in this direction, it is clear, that templates based on PS can offer new solutions for progress on the way to fabricate new functional nanomaterials.

Acknowledgements. The authors would like to thank L. Dolgiy and V. Tsybulskiy for their help during some works mentioned in this review. The research has been carried out in parts within the Grant X14MB-008 of the Belarusian Found for Fundamental Research, the Projects No 1.1.14 and No 2.3.06 financed by the State Program of Scientific Research of Belarus "Electronics and Photonics".

References

- [1] R. Herino, Nanocomposite materials from porous silicon, *Materials Science and Engineering: B* 69 (2000) 70-76.
- [2] H. Bandarenka, M. Balucani, R. Crescenzi, A. Ferrari, Formation of composite nanostructures by corrosive deposition of copper into porous silicon, *Superlattices and Microstructures* 44 (2008) 583-587.
- [3] E.B. Chubenko, A.A. Klyshko, V.A. Petrovich, V.P. Bondarenko, Electrochemical deposition of zinc selenide and cadmium selenide onto porous silicon from aqueous acidic solutions, *Thin Solid Films* 517 (2009) 5981-5987.
- [4] P. Granitzer, K. Rumpf, Porous Silicon - A Versatile Host Material, *Materials* 3 (2010) 943-998.
- [5] A. Dolgiy, S.V. Redko, H. Bandarenka, S.L. Prischepa, K. Yanushkevich, P. Nenzi, M. Balucani, V. Bondarenko, Electrochemical Deposition and Characterization of Ni in Mesoporous Silicon, *J. Electrochem. Soc.* 159 (2012) D623-D627.
- [6] S.L. Prischepa, A.L. Dolgiy, H.V. Bandarenka, V.P. Bondarenko, K.I. Yanushkevich, V.G. Bayev, A.A. Maximenko, Yu. A. Fedotova, A. Zarzycki, Y. Zabala, Synthesis and Properties of Ni Nanowires in Porous Silicon Templates, in *Nanowires: Synthesis, Electrical Properties and Uses in Biological Systems* (ed. Luke J. Wilson), Nova Science Publ. Inc., 2014, pp. 89-128.
- [7] L. Canham, *Handbook of Porous Silicon*, Springer International Publishing Switzerland, 2014.
- [8] Yu. Panarin, S. Terekhov, K. Kholostov, V. Bondarenko, SERS-active substrates based on n-type porous silicon, *Appl. Surf. Sci.* 256 (2010) 6969-6976.
- [9] H. Bandarenka, S. Redko, A. Smirnov, A. Panarin, S. Terekhov, P. Nenzi, M. Balucani, V. Bondarenko, Nanostructures formed by displacement of porous silicon with copper: from nanoparticles to porous membranes, *Nanoscale Res. Lett.* 7 (2012) 477-486.
- [10] C. Cirillo, M. Trezza, F. Chiarella, A. Vecchione, V. P. Bondarenko, S.L. Prischepa, C. Attanasio, Quantum phase slips in superconducting Nb nanowire networks deposited on self-assembled Si templates, *Appl. Phys. Lett.* 101 (2012) 172601-5.
- [11] A. Dolgiy, S. Redko, H. Bandarenka, A. Shapel, V. Bondarenko, Beta-battery based on ⁶³Ni/macroporous silicon, ECS Meeting Abstracts, Honolulu PRiME 2012, 7-12 October 2012 Honolulu, Hawaii, 359.
- [12] H. Bandarenka, K. Artsemyeva, S. Redko, A. Panarin, S. Terekhov, V. Bondarenko, Effect of swirl-like resistivity striations in n+-type Sb doped Si wafers on the properties of Ag/porous silicon SERS substrates, *Phys. Status Solidi C* 10 (2013) 624-627.
- [13] H. Bandarenka, S.L. Prischepa, R. Fittipaldi, A. Vecchione, P. Nenzi, M. Balucani, V. Bondarenko, Comparative study of initial stages of copper immersion deposition on bulk and porous silicon, *Nanoscale Res. Lett.* 8 (2013) 85-92.

- [14] C. Cirillo, S. Prischeva, M. Trezza, V. Bondarenko, C. Attanasio, Superconducting nanowire quantum interference device based on Nb ultrathin films deposited on self-assembled porous Si templates, *Nanotechnology* 25 (2014) 425205-14.
- [15] K. Artsemyeva, A. Dolgiy, H. Bandarenka, A. Panarin, I. Khodasevich, S. Terekhov, V. Bondarenko, Fabrication of SERS-active Substrates by Electrochemical and Electroless Deposition of Metals in Macroporous Silicon, *ECS Transactions* 53 (2013) 85-95.
- [16] K. Girel, H. Bandarenka, L. Dolgyi, Deposition of Silver Dendrites on Porous Silicon for Fabrication of SERS-active Substrates, in *Physics, Chemistry and Application of Nanostructures*, World Scientific Publishing Co. Pte. Ltd, Singapore, 2015, pp. 600-603.
- [17] P. Allongue, Porous Silicon Formation Mechanisms, in *Properties of Porous Silicon*, INSPEC, London, 1997, pp. 3-11.
- [18] R. Herino, Pore Size Distribution in Porous Silicon, in *Properties of Porous Silicon*, INSPEC, London, 1997, pp. 89-96.
- [19] N.I. Kargin, A.O. Sultanov, A.V. Bondarenko, V.P. Bondarenko, S.V. Red'ko, A.S. Ionov, Formation and Structure of Mesoporous Silicon, *Russian Microelectronics*, 43, 8 (2014) 531-535.
- [20] A. Loni, Porous Silicon Formation by Anodization, in *Handbook of Porous Silicon*, Springer International Publishing Switzerland, 2014, pp. 11-22.
- [21] A.Yu. Panarin, K.V. Girel, H.V. Bandarenka, I.A. Khodasevich, V.P. Bondarenko, S.N. Terekhov, Formation of Silver Nanostructures on Porous Silicon and Review of their Application, *Proceedings of the 2nd International Conference on Modern Applications of Nanotechnology*, Minsk, Belarus, 6-8 May 2015, S306.
- [22] A.V. Bondarenko, Chemical corrosive deposition of copper on porous silicon, in *Chemistry and Application of Nanostructures*, World Scientific Publishing Co. Pte. Ltd, Singapore, 2005, pp. 435-438.
- [23] H. Bandarenka, A. Shapel, M. Balucani, Cu-Si nanocomposites based on porous silicon matrix, *Solid State Phenomena* 151 (2009) 222-226.
- [24] H. Bandarenka, S. Redko, P. Nenzi, M. Balucani, V. Bondarenko, Optimization of chemical displacement deposition of copper on porous silicon, *J. Nanosci. Nanotechnol.* 12 (2012) 8725-8731.
- [25] H. Bandarenka, V. Tsubulskii, M. Balucani, V.P. Bondarenko, Chemical resistance of mesoporous silicon under immersion deposition of copper, in *Materials of the 9th International Conference on Porous Semiconductors – Science and Technology*, 9-14 March, 2014, Alicante, Spain, Craficas Cervantes, C.B., 2014, pp. 400-401.
- [26] A. Dolgiy, H. Bandarenka, V. Petrovich. Influence of Si conductivity type on immersion deposition of Cu films on porous Si, in *Physics, Chemistry and Application of Nanostructures*, World Scientific Publishing Co. Pte. Ltd, Singapore, 2015, pp. 280-283.
- [27] K.Y. Arutyunov, D.S. Golubev, A. D. Zaikin, Superconductivity in one dimension, *Phys. Rep.* 464 (2008) 1-70.
- [28] A. Bezryadin, Quantum suppression of superconductivity in nanowires, *J. Phys.: Condens. Matter* 20 (2008) 043202-18.
- [29] O.V. Astafiev, L.B. Ioffe, S. Kafanov, Yu.A. Pashkin, K.Yu. Arutyunov, D. Shahar, O. Cohen, J.S. Tsai, Coherent quantum phase slip, *Nature*, 484 (2012) 355-358.
- [30] J. Ku, V. Manucharyan, A. Bezryadin, Superconducting nanowires as nonlinear inductive elements for qubits, *Phys. Rev. B* 82 (2010) 134518-134528.
- [31] J. E. Mooij, Yu. V. Nazarov, Superconducting nanowires as quantum phase-slip junctions, *Nat. Phys.* 2 (2006) 169-172.
- [32] N. Giordano, Dissipation in a one-dimensional superconductor: Evidence for macroscopic quantum tunneling, *Phys. Rev. B* 41, 10 (1990) 6350-6365.

- [33] A. T. Bollinger, A. Rogachev, M. Remeika, A. Bezryadin, Effect of morphology on the superconductor-insulator transition in one-dimensional nanowires, *Phys. Rev. B* 69 (2004) 180503-06.
- [34] R.S. Newbower, M.R. Beasley, M. Tinkham, Fluctuation Effects on the Superconducting Transition of Tin Whisker Crystals, *Phys. Rev. B* 5 (1972) 864-868.
- [35] J. Wang, X.-C. Ma, L. Lu, A.-Z. Jin, C.-Z. Gu, X. C. Xie, J.-F. Jia, X. Chen, Q.-K. Xue, Anomalous magnetoresistance oscillations and enhanced superconductivity in single-crystal Pb nanobelts, *Appl. Phys. Lett.* 92, 233119-21 (2008).
- [36] A. Bezryadin, C. N. Lau, and M. Tinkham, Quantum suppression of superconductivity in ultrathin nanowires, *Nature* 404 (2000) 971-974.
- [37] D.S. Hopkins, D. Pekker, P.M. Goldbart, A. Bezryadin, Quantum interference device made by DNA templating of superconducting nanowires, *Science* 308 (2005) 1762-1765.
- [38] A. Bezryadin, P.M. Goldbart, Superconducting Nanowires Fabricated Using Molecular Templates, *Adv. Mater.* 22 (2010) 1111-1121.
- [39] S. Michotte, L. Piraux, S. Dubois, F. Pailloux, G. Stenuit, J. Govaerts, Superconducting properties of lead nanowires arrays, *Physica C* 377 (2002) 267-276.
- [40] Q. Luo, X. Q. Zeng, M. E. Mischczak, Z. L. Xiao, J. Pearson, T. Xu, W.K. Kwok, Phase slippage driven dissipation and high-field Little-Parks effect in superconducting MoGe nanowire networks formed on nanoporous substrates, *Phys. Rev. B* 85 (2012) 174513-19.
- [41] A. D. Zaikin, D.S. Golubev, A. van Otterlo, G.T. Zimanyi, Quantum phase slips and transport in ultrathin superconducting wires, *Phys. Rev. Lett.* 78 (1997) 1552-1555.
- [42] M.-H. Bae, R. C. Dinsmore III, T. Aref, M. Brenner, and A. Bezryadin, Current-Phase Relationship, Thermal and Quantum Phase Slips in Superconducting Nanowires Made on a Scaffold Created Using Adhesive Tape, *Nano Lett.* 9 (2009) 1889-1896.
- [43] M. Fleischmann, P.J. Hendra, A.J. McQuillan, Raman spectra of pyridine adsorbed at a silver electrode, *Chem. Phys. Lett.* 26 (1974) 163-166.
- [44] D.L. Jeanmaire, R.P. Van Duyne, Surface Raman spectroelectrochemistry: 1. Heterocyclic, aromatic, and aliphatic-amines adsorbed on anodized silver electrode, *J. Electroanal. Chem.* 84 (1977) 1-20.
- [45] M.G. Albrecht, J.A. Creighton, Anomalous intense Raman-spectra of pyridine at a silver electrode, *J. Am. Chem. Soc.* 99 (1977) 5215-5217.
- [46] S.C. Ponzaru, I. Pavel, N. Leopold, W. Kiefer, Identification and characterization of pharmaceuticals using Raman and surface-enhanced Raman scattering, *J. Raman Spectrosc.* 35 (2004) 338-346.
- [47] J.M. Reyes-Goddard, H. Barr, N. Stone, Photodiagnosis using Raman and surface enhanced Raman scattering of bodily fluids, *Photodiag. Photodyn. Ther.* 2 (2005) 223-233.
- [48] J. Kneipp, H. Kneipp, K. Kneipp, SERS—a single-molecule and nanoscale tool for bioanalytics, *Chem. Soc. Rev.* 37 (2008) 1052-1060.
- [49] K. Hering, D. Cialla, K. Ackermann, T. Dorfer, R. Moller, H. Schneidewind, R. Mattheis, W. Fritzsche, P. Rosch, J. Popp, SERS: a versatile tool in chemical and biochemical diagnostics, *Anal. Bioanal. Chem.* 390 (2008) 113-124.
- [50] K. Kneipp, Y. Wang, H. Kneipp, I. Itzkan, R.R. Dasari, M.S. Feld, Population pumping of excited vibrational states by spontaneous surface-enhanced Raman scattering, *Phys. Rev. Lett.* 76 (1996) 2444-2447.
- [51] S. Nie, S.R. Emory, Probing single molecules and single nanoparticles by surface-enhanced Raman scattering, *Science* 275 (1997) 1102-1106.
- [52] K. Kneipp, H. Kneipp, G. Deinum, I. Itzkan, R.R. Dasari, M.S. Feld, Single-molecule detection of a cyanine dye in silver colloidal solution using near-infrared surface-enhanced Raman scattering, *Appl. Spectrosc.* 52 (1998) 175-178.

- [53] C.L. Haynes, R.P. Van Duyne, Nanosphere lithography: a versatile nanofabrication tool for studies of size-dependent nanoparticle optics, *J. Phys. Chem. B* 105 (2001) 5599-5611.
- [54] N. Felidj, J. Aubard, G. Levi, J.R. Krenn, M. Salerno, G. Schider, B. Lamprecht, A. Leitner, F.R. Aussenegg, Controlling the optical response of regular arrays of gold particles for surface-enhanced Raman scattering, *Phys. Rev. B* 65 (2002) 075419.
- [55] J.C. Hulteen, R.P. Van Duyne, Nanosphere lithography: a materials general fabrication process for periodic particle array surfaces, *J. Vac. Sci. Technol. A* 13 (1995) 1553-1558.
- [56] L. Baia, M. Baia, J. Popp, S. Astilean, Gold films deposited over regular arrays of polystyrene nanospheres as highly effective SERS substrates from visible to NIR, *J. Phys. Chem. B* 110 (2006) 23982-86.
- [57] S. Chan, S. Kwon, T.-W. Koo, P.L. Lee, A.A. Berlin, Surface-enhanced Raman scattering of small molecules from silver-coated silicon nanopores, *Adv. Mater.* 15 (2003) 1595-1598.
- [58] H. Lin, J. Mock, D. Smith, T. Gao, M.J. Sailor, Surface-enhanced Raman scattering from silver-plated porous silicon, *J. Phys. Chem. B* 108 (2004) 11654-11659.
- [59] F. Giorgis, E. Descrovi, A. Chiodoni, E. Froner, M. Scarpa, A. Venturello, F. Geobaldo, Porous silicon as efficient surface enhanced Raman scattering (SERS) substrate, *Appl. Surf. Sci.* 254 (2008) 7494-7497.
- [60] A. Yu. Panarin, V. S. Chirvony, K. I. Kholostov, P.-Y. Turpin, S. N. Terekhov, Formation of SERS-Active Silver Structures on the Surface of Mesoporous Silicon, *J. Appl. Spectroscopy* 76, 2 (2009) 281-287.
- [61] S. N. Terekhov, P. Mojzes, S. M. Kachan, N. I. Mukhurov, S. P. Zhvavyi, A. Yu. Panarin, I. A. Khodasevich, V. A. Orlovich, A. Thorel, F. Grillond, P.-Y. Turpin, A comparative study of surface-enhanced Raman scattering from silver-coated anodic aluminum oxide and porous silicon, *J. Raman Spectrosc.* 42 (2011) 12-20.
- [62] T. A. Kelf, Y. Sugawara, R. M. Cole, J. J. Baumberg, Localized and delocalized plasmons in metallic nanovoids, *Phys. Rev. B* 74, (2006) 245415-12.
- [63] N. D. Denkov, O. D. Veleev, P. A. Kralchevsky, I. B. Ivanov, H. Yoshimura and K. Nagayama, Mechanism of formation of two-dimensional crystals from latex particles on substrates, *Langmuir* 8, (1992) 3183-3190.
- [64] A. S. Dimitrov, K. Nagayama, Continuous Convective Assembling of Fine Particles into Two-Dimensional Arrays on Solid Surfaces, *Langmuir* 12 (1996) 1303-1311.
- [65] P. Jiang, J. F. Bertone, K. S. Hwang and V. L. Colvin, Single-Crystal Colloidal Multilayers of Controlled Thickness, *Chem. Mater.* 11 (1999) 2132-2140.
- [66] R. M. Cole, S. Mahajan, P. N. Bartlett, J. J. Baumberg, Engineering SERS via absorption control in novel hybrid Ni/Au nanovoids, *Optic Express* 17 (2009) 13298-13308.
- [67] H. Bandarenka, K. Girel, V. Lukashevich, V. Bondarenko, Determination of tear proteins by surface enhanced Raman scattering, Abstracts of Third International Conference on Advanced Complex Inorganic Nanomaterials, 13–17 July 2015, Namur, Belgium, 2015, P-180.
- [68] J.-M. Escoffre, T. Portet, L. Wasungu, J. Teissie, D. Dean, M.-P. Rols, What is (still not) known of the mechanism by which electroporation mediates gene transfer and expression in cells and tissues, *Molecular Biotechnology* 41 (2009) 286-295.
- [69] M. Balucani, P. Nenzi, C. Crescenzi, P. Marracino, F. Apollonio, M. Liberti, A. Densi, C. Colizzi, Technology and Design of Innovative Flexible Electrode for Biomedical Applications, *Electronic Components and Technology Conference*, 2011, pp. 1319-1324.